Brain abnormalities, defective meiotic chromosome synapsis and female subfertility in HSF2 null mice

Marko Kallio, Yunhua Chang, Martine Manuel, Tero-Pekka Alastalo, Murielle Rallu, Yorick Gitton, Lila Pirkkala, Marie-Thérèse Loones, Liliana Paslaru, Severine Larney, et al.

The EMBO Journal Vol. 21 No. 11 pp. 2591–2601, 2002

Brain abnormalities, defective meiotic chromosome synapsis and female subfertility in HSF2 null mice

Marko Kallio[1,2], Yunhua Chang[3], Martine Manuel[3,4], Tero-Pekka Alastalo[1], Murielle Rallu[3,5], Yorick Gitton[4], Lila Pirkkala[1], Marie-Thérèse Loones[3], Liliana Paslaru[3], Severine Larney[6], Sophie Hiard[6], Michel Morange[3,7], Lea Sistonen[1,8] and Valérie Mezger[3]

[1]Turku Centre for Biotechnology, University of Turku, Abo Akademi University, FIN-20520 Turku, [8]Department of Biology, Abo Akademi University, Turku, Finland, [3]UMR8541 and [6]Animal Facilities, Ecole Normale Supérieure, F-75230 Paris cedex 05, France

[2]Present address: Department of Cell Biology, University of Oklahoma Health Sciences Center, Oklahoma City, OK 73104, USA
[4]Present address: Department of Biomedical Sciences, University of Edinburgh, Edinburgh, UK
[5]Present address: Developmental Genetics Program, Skirball Institute for Biomolecular Medicine, NYU Medical Center, New York, NY 10016, USA

[7]Corresponding author
e-mail: morange@wotan.ens.fr

M.Kallio, Y.Chang and M.Manuel contributed equally to this work

Heat shock factor 2, one of the four vertebrate HSFs, transcriptional regulators of heat shock gene expression, is active during embryogenesis and spermatogenesis, with unknown functions and targets. By disrupting the *Hsf2* gene, we show that, although the lack of HSF2 is not embryonic lethal, *Hsf2*$^{-/-}$ mice suffer from brain abnormalities, and meiotic and gametogenesis defects in both genders. The disturbances in brain are characterized by the enlargement of lateral and third ventricles and the reduction of hippocampus and striatum, in correlation with HSF2 expression in proliferative cells of the neuroepithelium and in some ependymal cells in adults. Many developing spermatocytes are eliminated via apoptosis in a stage-specific manner in *Hsf2*$^{-/-}$ males, and pachytene spermatocytes also display structural defects in the synaptonemal complexes between homologous chromosomes. *Hsf2*$^{-/-}$ females suffer from multiple fertility defects: the production of abnormal eggs, the reduction in ovarian follicle number and the presence of hemorrhagic cystic follicles are consistent with meiotic defects. *Hsf2*$^{-/-}$ females also display hormone response defects, that can be rescued by superovulation treatment, and exhibit abnormal rates of luteinizing hormone receptor mRNAs.

Keywords: apoptosis/brain defects/gametogenesis/HSF2/synaptonemal complex

Introduction

Heat shock proteins (Hsps) function as molecular chaperones at various stages in protein biogenesis and degradation (Mathew and Morimoto, 1998). Hsps are induced following proteotoxic stresses and in a variety of physiopathological conditions (fever, ischemia, viral or bacterial infections, brain injury and aging). Hsps are also required for normal progression of the cell cycle and differentiation. Some HSPs are crucial in the maintenance of spermatogenesis (testis-specific Hsps; reviewed in Eddy, 1999) and for embryogenesis (see for example Voss *et al*., 2000).

Hsp gene transcription is regulated by heat shock factors (HSFs) (Pirkkala *et al*., 2001). In *Drosophila*, the sole HSF is necessary for larval development and oogenesis, independently of *hsp* gene expression (Jedlicka *et al*., 1997). In vertebrates, four HSFs are found. HSF1 is the major heat stress-responsive factor expressed ubiquitously. Like *Drosophila* HSF, HSF1 plays a role in development (McMillan *et al*., 1998; Xiao *et al*., 1999). Inactivation of the mouse *Hsf1* gene leads to placental insufficiency and growth retardation. *Hsf1*$^{-/-}$ females are infertile due to the fact that HSF1 is a maternal factor present in the one-cell stage embryo and is required for development to the two-cell stage (Christians *et al*., 2000). Male mice expressing an active form of HSF1 in the testis are infertile due to apoptosis of pachytene spermatocytes, while female fertility is not affected (Nakai *et al*., 2000).

In contrast to ubiquitous HSF1, HSF2 is expressed at high levels and is only active in two developmental pathways: spermatogenesis and embryogenesis. HSF2 mRNA and protein are expressed in a stage-specific manner during adult spermatogenesis in rodents, and the protein localizes to the nuclei of early pachytene spermatocytes and round post-meiotic spermatocytes (Sarge *et al*., 1994; Alastalo *et al*., 1998). In contrast to HSF1, HSF2 is not a maternal factor, but is active from the eight-cell stage (Mezger *et al*., 1994a,b) and peaks around day 9.5 of gestation, with elevated levels in the developing neural tube. HSF2 levels and activity then decrease and are restricted to the developing brain in E15.5 embryos (Rallu *et al*., 1997). HSF2 function and targets have remained obscure, with no clear correlations with Hsp expression. Here, we have investigated the role of HSF2 by inactivating the mouse *Hsf2* gene using homologous recombination.

Results

Targeted disruption of the Hsf2 gene in ES cells and generation of HSF2-deficient mice

Since HSF2 is expressed in embryonic stem (ES) cells, we chose a promoterless targeting vector strategy to disrupt the *Hsf2* gene, by insertion of the β-*geo* gene in-phase at the *Sph*I site of exon 5, which lies in the oligomerization domain of HSF2. In the case of a homologous recombination event, a chimeric protein is produced, which retains the HSF2 DNA-binding domain, but is interrupted in the oligomerization domain at Lys167: the first hydrophobic array of six heptad repeats is conserved, but the overlap-

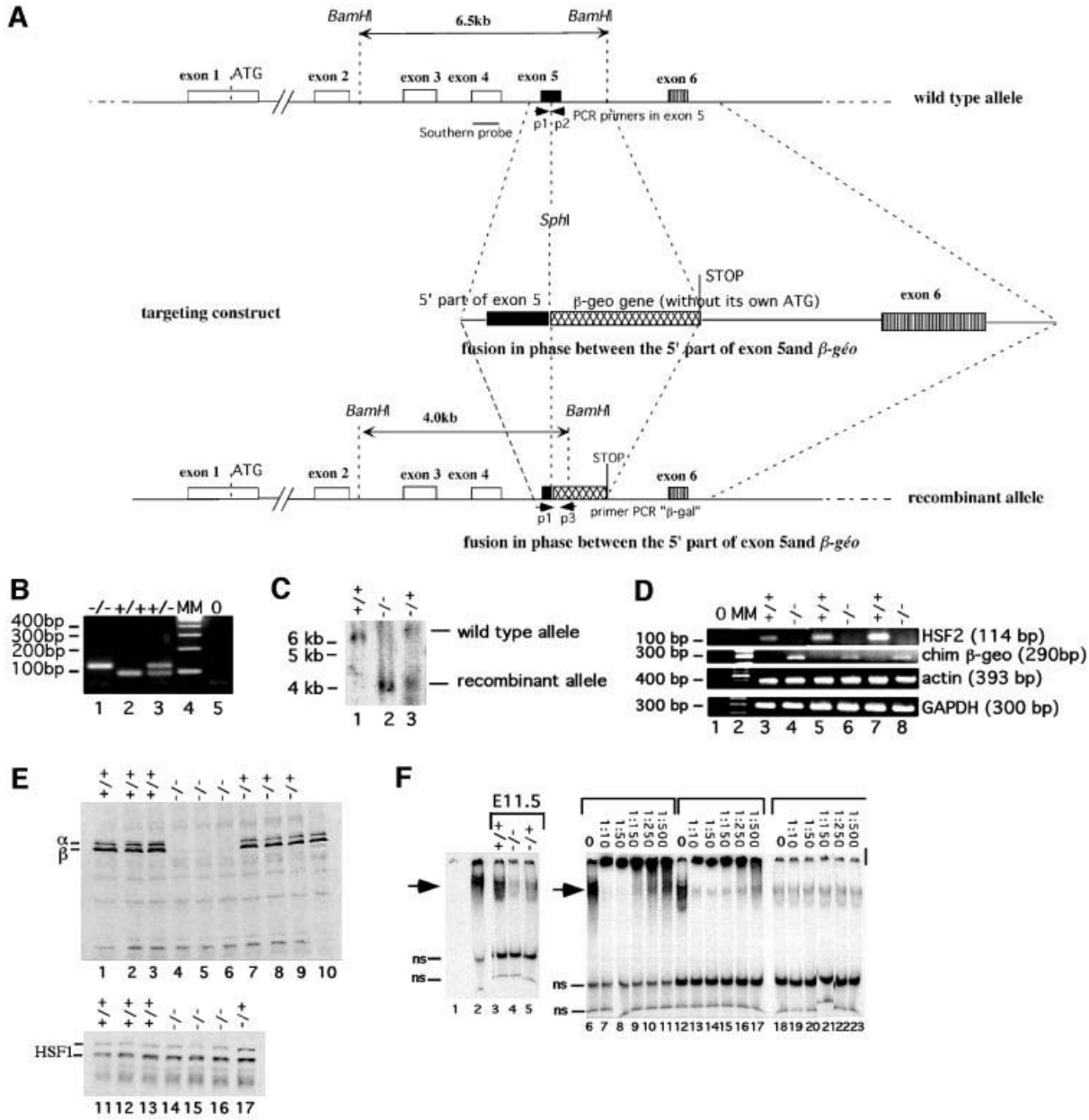

Fig. 1. Targeted inactivation of the *Hsf2* gene. (**A**) Schematic representation of the wild-type and mutated alleles. Horizontal small arrows show the location of the three primers used for PCR genotyping. (**B**) PCR genotyping of offspring from F_1 heterozygous intercrosses. (**C**) Southern blot of *Bam*HI-digested tail DNA. Lanes 1 and 3: wild-type allele 6.5 kb fragment. Lanes 2 and 3: disrupted allele 4 kb fragment. (**D**) RT–PCR analysis of HSF2, chimeric HSF2-βgeo, actin and GAPDH mRNA levels in *Hsf2*$^{+/+}$, *Hsf2*$^{+/-}$ and *Hsf2*$^{-/-}$ tissues. Lane 1: no reverse transcription (0); lane 2, molecular markers (MM); lanes 3 and 4, testis; lanes 5 and 6, E9.5 embryos; lanes 7 and 8, E13.5 embryos. (**E**) Western blot analysis of whole E11.5 embryo extracts of littermates with polyclonal anti-mouse HSF2 (upper panel). Equal loading and transfer were assessed with a monoclonal anti-HSF1 (lower panel). Lanes 1–3 and 11–13, *Hsf2*$^{+/+}$; lanes 4–6 and 14–17, *Hsf2*$^{-/-}$; lanes 7–9 and 17, *Hsf2*$^{+/-}$; lane 10, unstressed F9 EC cells. (**F**) EMSA analysis of E11.5 embryo extracts with an HSE-containing double-stranded oligonucleotide. Lane 1, no extracts; lanes 2 and 6–11, unstressed F9 EC cells; lanes 3–5 and 12–23, embryos. The dilutions of polyclonal anti-mouse HSF2 in supershift experiment are indicated. Arrowheads, specific HSF2–HSE complexes; ns, non-specific complexes.

ping arrays 2 and 3 are eliminated (Wu, 1995). Therefore, the expected chimeric protein cannot trimerize or bind DNA (Figure 1A). Moreover, this protein lacks NLS2, one of the two HSF2 nuclear localization signals, which lies between the residues Lys195 and Lys210. Since both NLS are necessary for the nuclear localization of HSF2, the chimeric protein is expected to be cytoplasmic and not able to perform nuclear functions (Sheldon and Kingston, 1993). The homologous recombination places the β-*geo* gene in-phase with the beginning of exon 5 and without a promoter in the targeting construct. The β-*geo* gene is a chimera between the *lacZ* gene and the G418 resistance gene (*neo*) (Friedrich and Soriano, 1991). After electroporation with the targeting vector, the G418-resistant ES clones result either from rare random insertion of the targeting construct, in-phase with a promoter, or from homologous recombination, which places the β-*geo* gene under the control of the *Hsf2* promoter region, active in ES

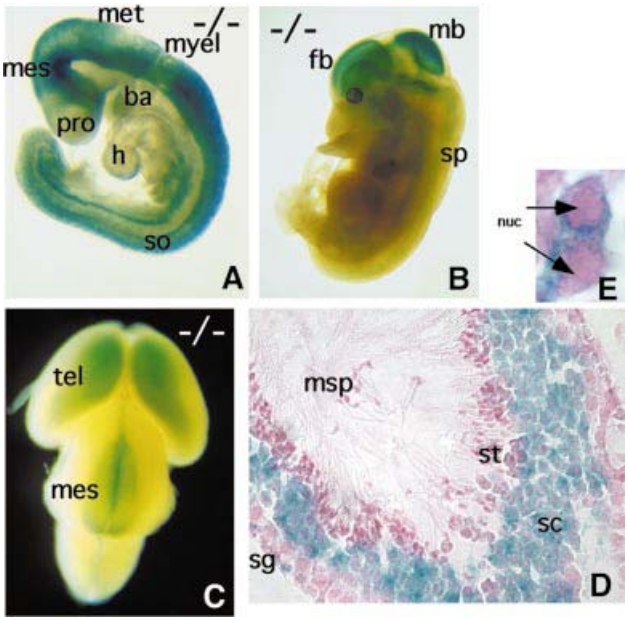

Fig. 2. *LacZ* expression as a reporter of the HSF2 expression profile. (**A** and **B**) Lateral view of an E9.5 and E13.5 *Hsf2*$^{-/-}$ embryo, respectively. (**C**) Dorsal view of an E15.5 *Hsf2*$^{-/-}$ embryo. (**D**) Transverse section of a seminiferous tubule showing X-gal staining of spermatocytes. (**E**) Cytoplasmic localization of the chimeric recombinant protein using β-galactosidase detection by X-gal staining (blue) in mouse pachytene spermatocytes (*Hsf2*$^{-/-}$ male). nuc, nucleus; h, heart; so, somites; pro, prosencephalon; mes, mesencephalon; met, metencephalon; myel, myelencephalon; tel, telencephalon; ba, branchial arches; fb, forebrain; mb, midbrain; sp, spinal chord; msp, mature spermatozoa; sg, spermatogonia; sc, spermatocytes; st, spermatids.

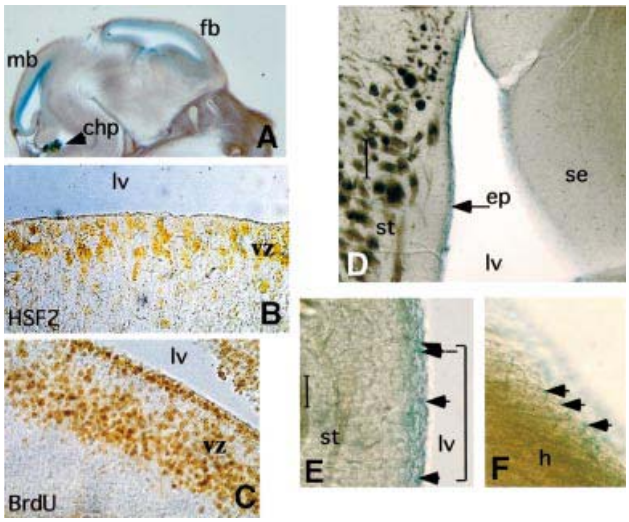

Fig. 3. HSF2 and β-gal expression in the ventricular zone of embryonic and adult brain. (**A**) Parasagittal section of an E13.5 *Hsf2*$^{-/-}$ embryonic brain showing β-gal expression along the lumen of the ventricles. fb, forebrain; mb, midbrain; chp, choroid plexus. (**B** and **C**) HSF2 immunolocalization and BrdU staining, respectively, at the level of midbrain in E12.5 *Hsf2*$^{+/+}$ embryos. vz, ventricular zone; lv, lumen of the ventricle. (**D**–**F**) β-gal detection in the ependymal layer of adult *Hsf2*$^{-/-}$ brain. st, striatum; se, septum; ep, ependymal zone; lv, lateral ventricle. Scale bar: 50 μm. (E) Detail of (D), magnification: 20×. (F) Detail of a transverse section at the level of the hippocampus (h), magnification: 20×.

cells. After recombination in ES cells, the β-galactosidase expression is the reporter of the *Hsf2* promoter activity.

Recombination events at the *Hsf2* locus were identified among the G418-resistant colonies by Southern blot analysis of ES cell genomic DNA with a 5′-external probe. Among 27 colonies, two showed a Southern pattern compatible with recombination of one *Hsf2* allele and were used for injection into C57Bl/6 blastocysts. One of them led to germline transmission. One female chimera was obtained and crossed with C57Bl/6 males. The presence of a wild-type or mutated *Hsf2* allele in progeny was determined by PCR amplification and confirmed by Southern blot (Figure 1B and C).

F_1 heterozygous (*Hsf2*$^{+/-}$; C57Bl/6/129Sv genetic background) mice were viable and intercrossed. Litter size for these intercrosses was normal (8.6 ± 2.3 pups/litter, $n = 15$). Out of 132 genotyped F_2 progeny, 30 were wild type (22.7%), 69 heterozygous (52.3%) and 33 homozygous (25%), not statistically different from a Mendelian rate (25, 50 and 25%). A similar male:female ratio was observed (17 females for 13 males in wild-type individuals; 35 males and 34 females for heterozygotes; and 14 males and 19 females for homozygotes).

To confirm that *Hsf2*-null mutants were devoid of wild-type HSF2, we measured the HSF2 mRNA levels by RT–PCR on adult testis and on E9.5 and E13.5 embryos. No HSF2 mRNA was detected in the samples from *Hsf2*$^{-/-}$ testis or embryos (Figure 1D). In contrast, the chimeric recombinant mRNA encoding β-geo was detected in *Hsf2*$^{-/-}$ testis and embryos, but not in the wild-type samples. Western blot analysis confirmed the absence of HSF2 protein in *Hsf2*$^{-/-}$ embryos (Figure 1E) and testes (data not shown). To exclude the fact that the chimeric recombinant protein could retain HSE-binding activity, even as a monomer, we performed electrophoretic mobility shift assay (EMSA) on E11.5 embryo whole extracts. F9 embryonal carcinoma (EC) cells, which contain high levels of active HSF2, were used as positive controls. In *Hsf2*$^{+/-}$ embryos, constitutive HSE-binding activity was reduced notably when compared with wild types (Figure 1F, lanes 3 and 5). A faint signal was detected in the *Hsf2*$^{-/-}$ embryos (Figure 1F, lane 4), but this residual HSE-binding activity was not due to HSF2. Indeed, an antibody able to induce total supershift of HSF2 complexes in F9 EC cells (Figure 1F, lanes 6–11) did not induce any supershift of the HSE complexes present in *Hsf2*$^{-/-}$ extracts, even at high concentrations (Figure 1F, lanes 18–23). A similar residual HSE-binding activity remained in wild-type embryos after supershifting with anti-HSF2 (Figure 1F, lanes 13–17). X-gal staining on testis (Figure 2E) and brain (data not shown), and immunohistochemistry on embryonic fibroblasts (data not shown), confirmed that the chimeric protein was cytoplasmic and not nuclear, suggesting that it cannot reach any DNA targets, even if it may retain a minor DNA-binding activity, undetectable by EMSA. We conclude that HSF2 deficiency was not embryonic lethal and that the phenotype associated with the homozygous mutation, as described below, is due to the lack of functional HSF2 protein.

The lacZ reporter gene expression faithfully reproduces the HSF2 expression profile

We analyzed the β-galactosidase (β-gal) expression pattern, a reporter of *Hsf2* promoter activity in embryos and adults. At all embryonic stages, the overall pattern of β-gal expression was similar in $Hsf2^{+/-}$ and $Hsf2^{-/-}$ embryos, except for signal intensity. As expected, no β-gal activity was detected in one-cell stage embryos (Mezger *et al*., 1994a,b; Christians *et al*., 1997). At E7.5, all three embryonic layers were highly stained, and at E8.5 the head fold was marked more strongly (data not shown). At E9.5, the β-gal expression was very strong in the developing nervous system, but absent from the trunk mesenchyme (Figure 2A). At E13.5, the β-gal activity was restricted to the central nervous system (CNS) (Figure 2B) and, at E15.5, this pattern was even more restricted within the telencephalic vesicles and part of the midbrain (Figure 2C). The β-gal activity profile was restrained progressively to the developing CNS and therefore parallels HSF2 DNA-binding activity profiles (Rallu *et al*., 1997).

In adults, strong β-gal activity was detected in the spermatocytes (Figure 2D), a known site of HSF2 expression during spermatogenesis (Sarge *et al*., 1994; Alastalo *et al*., 1998), but not in the elongated spermatids or spermatozoa. Sertoli cells did not express β-gal, but type A spermatogonia were stained.

Characteristics of HSF2 expression in the developing and adult brain

In the developing brain, β-gal was not expressed in the whole neuroepithelium, but was restricted along the lumen of the ventricles (Figure 3A). The ventricular zone (vz) is the location of the proliferating neural precursors (Takahashi *et al*., 1992). Comparison at E12.5 of the HSF2 profile, detected by immunohistochemistry, and of the proliferating cells of the vz, stained by anti-bromodeoxyuridine (BrdU) antibodies, confirmed that HSF2 expression corresponds to proliferating cells in the vz (Figure 3B and C). High magnification revealed that HSF2 staining was mainly nuclear and seemed to exclude the S phase cells (BrdU-positive cells located to the internal vz). Interestingly, β-gal expression was also detected at specific sites in the adult brain: in some discrete cells of the ependymal layer near the vz (Figure 3D–F).

Structural abnormalities and β-galactosidase expression in the adult brain

The HSF2 and β-gal expression patterns in proliferative regions of the developing brain prompted us to investigate the effects of HSF2 deficiency in the adult brain. $Hsf2^{-/-}$ adult brains (n = 9) systematically displayed structural abnormalities when compared with wild-type brains (n = 7); the lateral and third ventricles were enlarged and the hippocampus was dramatically reduced at all parasagittal or transverse section levels in adult brain (Figure 4).

Alteration of spermatogenesis in $Hsf2^{-/-}$ males

Seminiferous tubules of homozygous $Hsf2^{-/-}$ mice exhibit morphological changes. Testes in $Hsf2^{-/-}$ mice were significantly smaller ($P < 0.01$) than in wild-type animals

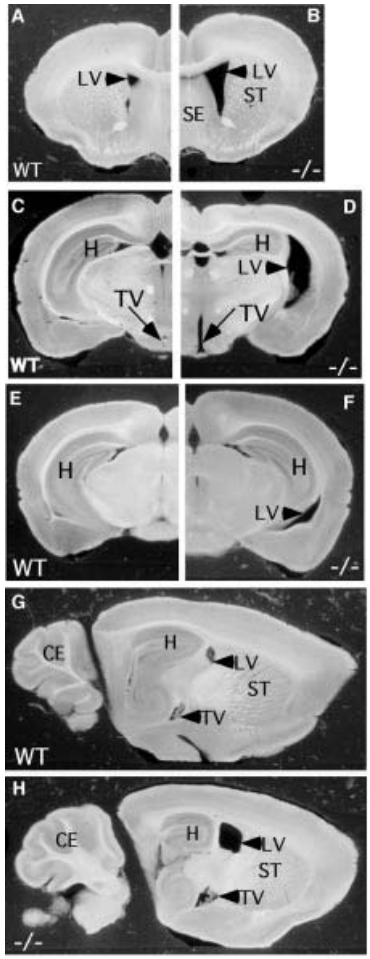

Fig. 4. Abnormal structure of the HSF2-deficient adult brain. Brain transverse sections (A–F) from $Hsf2^{+/+}$ (**A**, **C** and **E**) or $Hsf2^{-/-}$ (**B**, **D** and **F**) 3-month-old males, illustrating the enlargment of the lateral and third ventricles all along the brain. (**G** and **H**) Parasagittal sections of the adult brain showing the reduced size of the hippocampus in $Hsf2^{-/-}$ (–/–) (H) compared with $Hsf2^{+/+}$ (WT) (G) brain. ST, striatum; SE, septum; H, hippocampus; LV, lateral ventricle; TV, third ventricle; CE, cerebellum.

(Figure 5A). The mean weight of testes isolated from the $Hsf2^{-/-}$ animals was 70.4 ± 7.1 mg versus 113.1 ± 4.7 mg for wild-type testes. The average diameter of seminiferous tubules in the HSF2-deficient testis (n = 5 mice, 165.5 ± 28.7 μm) was significantly smaller ($P < 0.01$) than in $Hsf2^{+/+}$ mice (n = 5 mice, 187.3 ± 16.2 μm). Microscopic analysis of hematoxylin- and eosin-stained testis sections revealed that the $Hsf2^{+/+}$ animals had tubules containing normal amounts of differentiating germ cells from different developmental steps organized into the typical layer pattern (Figure 5B). In the $Hsf2^{-/-}$ mice, however, many of the tubules showed signs of disruption of spermatogenesis such as degenerating cells with condensed nuclei and eosin-positive cytoplasm, absence of certain differentiating spermatocytes and spermatids, and vacuolization of the tubules. Occasionally, tubules devoid of all meiotic spermatocytes and post-meiotic haploid spermatids were observed (Figure 5B). In addition, the average weight of the epididymis of $Hsf2^{-/-}$ mice was less than for wild-type animals (data not shown). The number of sperm found in

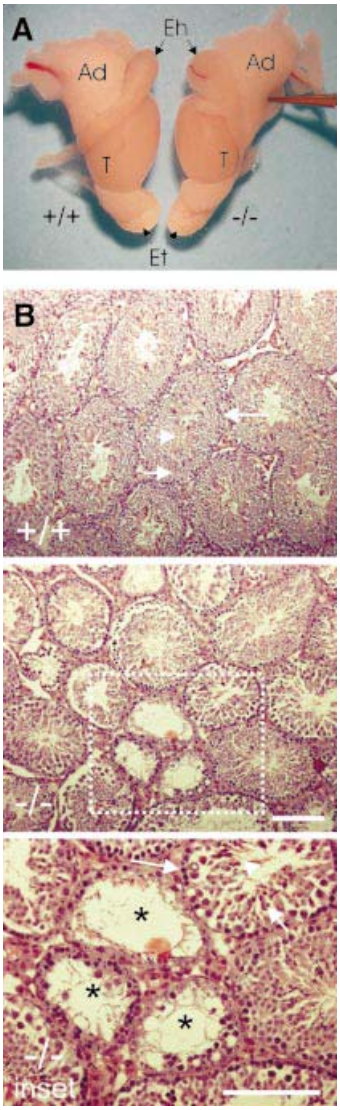

Fig. 5. Gross anatomy of male reproductive organs and analysis of testis cross-sections of adult *Hsf2*$^{+/+}$ (+/+) and *Hsf2*$^{-/-}$ mice (–/–). (**A**) Testis and epididymis size. T, testis; Eh, head of epididymis; Et, tail of epididymis; Ad, adipose tissues. (**B**) Cross-sections from testes. For (+/+): arrowhead, elongating spermatids; short arrow, spermatocytes; long arrow, spermatogonia. For (–/–): reduction in the diameter of the seminiferous tubules and indications of disruption of spermatogenesis. For inset: lack of spermatocytes (short arrow) and spermatids (arrowhead), vacuolization of the tubules (asterisk). Bars = 100 μm.

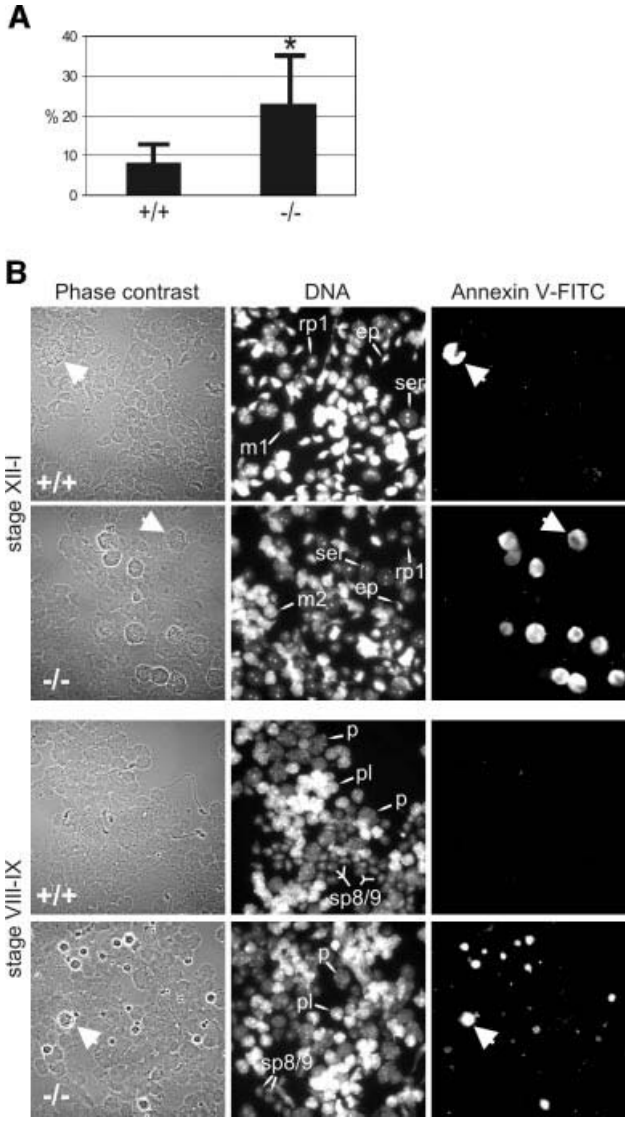

Fig. 6. Apoptosis of developing germ cells in the testes of *Hsf2*$^{-/-}$ mice. (**A**) Flow cytometric analysis of annexin V–FITC-stained testicular cells. (**B**) Stage-specific apoptosis in the testis of *Hsf2*$^{-/-}$ mice. Translumination-assisted dissection of the seminiferous tubules followed by annexin V–FITC immunofluorescence and microscopic analysis revealed two populations of dying cells in the *Hsf2*$^{-/-}$ mice at stages VIII–IX and XII–I; late pachytene and meiotically dividing spermatocytes (arrows). Tubule segments isolated from stages XII–I containing type A3 and A4 spermatogonia, early pachytene spermatocytes, meiotically dividing spermatocytes (m1, m2), round step-1 spermatids (rp1) and elongating spermatids (ep), and from stages VIII–IX containing type A1 spermatogonia, pre-leptotene spermatocytes (pl), late pachytene spermatocytes (p) and elongating step-8/9 spermatids (sp8/9). Note the reduction in the number of post-meiotic round and elongated spermatids in the *Hsf2*$^{-/-}$ mice.

the epididymis of the *Hsf2*$^{-/-}$ mice ($n = 5$, $7.9 \pm 6.5 \times 10^6$ per ml of the isolation buffer) was significantly lower ($P < 0.05$), in comparison with sperm counts of *Hsf2*$^{+/+}$ animals ($n = 5$, $18.6 \pm 11.7 \times 10^6$ per ml of the isolation buffer).

Increased apoptosis in the testes of Hsf2$^{-/-}$ *mice*. We isolated all testicular cells and performed staining with fluorescein isothiocyanate (FITC)-conjugated annexin V, a method used successfully in the detection of apoptosis in testis and other organs by flow cytometry and on tissue sections (Vermes *et al*., 1995; Henriksen and Parvinen, 1998; van Engeland *et al*., 1998). Flow cytometric analysis of whole testis cells from *Hsf2*$^{-/-}$ and *Hsf2*$^{+/+}$ animals showed a significant difference ($P < 0.05$) in the number of annexin V–FITC-positive cells: $22.6 \pm 12.1\%$ of the cells in the testes of *Hsf2*$^{-/-}$ mice ($n = 5$) were annexin V–FITC-positive compared with $8.1 \pm 4.1\%$ of the *Hsf2*$^{+/+}$ mice ($n = 5$, Figure 6A). Clusters of apoptotic cells were detected by TUNEL assay within the seminiferous tubules of *Hsf2*$^{-/-}$ males (data not shown).

Spermatocytes of the HSF2-deficient mice die at late pachytene of meiotic prophase and during meiotic divisions. We investigated what types of cell undergo apoptosis in the testis by utilizing stage-specific microdissection of seminiferous tubules (Parvinen *et al*., 1993).

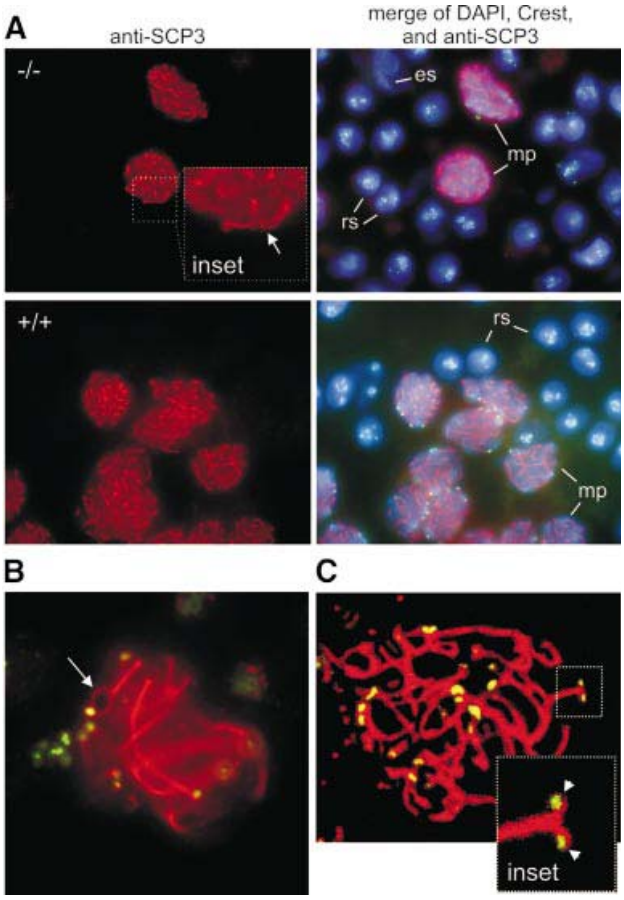

Fig. 7. Synapsis between the homologous chromosomes is defective in the *Hsf2*$^{-/-}$ mice. (**A**) Immunofluorescence labeling with anti-SCP3 antibody (Cy3 channel, red) and Crest anti-centromere sera (FITC channel, green). A part of a seminiferous tubule in developmental stage VIII (Clermont, 1972), with middle pachytene spermatocytes (mp), round spermatids (rs) and elongated spermatids (es). Loop-like configurations are present between one or more pairs of homologous chromosomes (arrow in the inset A). (**B**) An SC with one loop-like structure near the centromere terminus of a chromosome pair (arrow) (*Z*-level section). (**C**) Separation of the lateral elements at the centromere region (arrowheads in the inset C; stack of five *Z*-level sections from a confocal microscope series). Merge of anti-SCP3 (red) and Crest (green) in images (B) and (C). Bars = 10 μm.

Isolated cells from individual stages of spermatogenesis were fixed on slides and stained with annexin V–FITC. The dying cells in the *Hsf2*$^{-/-}$ mice testes were always found in clusters, indicating a stage-specific elimination of the cells during spermatogenesis. Two major annexin V–FITC-positive cell populations were discovered at stages VIII–IX and XII–I in the *Hsf2*$^{-/-}$ mice testes (Figure 6B). The spermatocytes at late pachytene of meiotic prophase and at meiotic divisions together accounted for almost 90% of the dying cells in *Hsf2*$^{-/-}$ testis. The 500 annexin V–FITC-positive cells analyzed from three *Hsf2*$^{-/-}$ mice were in early stages of apoptosis: 169 (34%) were at pachytene and 277 (55%) at meiotic M phase. The third apoptotic testicular cell type was type A spermatogonia that died at mitosis (data not shown). A few apoptotic cells were also detected in the *Hsf2*$^{+/+}$ animals (Figure 6B), most of which were late pachytene or meiotically dividing spermatocytes.

Synaptonemal complexes of pachytene spermatocytes are malformed in the Hsf2$^{-/-}$ *mice.* The synaptonemal complex (SC) forms the axis of paired chromosomes during the pachytene stage (Walker and Hawley, 2000). We investigated the structure of SCs in mid-pachytene spermatocytes of HSF2-deficient and wild-type mice using immunohistochemical detection of synaptonemal complex protein 3 (SCP3), which is localized in the lateral elements of the SC (Schalk *et al.*, 1998).

The structure of the SC in *Hsf2*$^{-/-}$ pachytene spermatocytes was often disorganized (Figure 7A). The continuous parallel alignment of the lateral elements was disrupted in 16.5% of the *Hsf2*$^{-/-}$ spermatocytes at stages VII–IX (33 cells of a total of 200 analyzed in four *Hsf2*$^{-/-}$ animals), corresponding to the mid-pachytene stage. In *Hsf2*$^{+/+}$ animals, only 3.5% of cells (seven cells of a total of 200 analyzed in two wild-type mice) had similar structural defects ($P < 0.05$). A typical cell with a defective SC had 1–4 pairs of lateral elements, along which one or a maximum of two loop-like structures were observed, indicative of defective synapsis between the pairs of homologous chromosomes (Figure 7B). The site of the loop-like structure varied along the SC from the very centromere-proximal end to the opposite end. In a few *Hsf2*$^{-/-}$ cells, the region of asynapsis was at the centromere terminus of the acrocentric mouse chromosome pairs, causing separation of the centromere pairs detected with Crest anti-centromere antisera (Figure 7C).

The impact of these defects on male fertility was investigated. Five wild-type males and five homozygous males were crossed over a 5 month period with four outbred OF1 females each. The averages of pups/litter, 9.30 ± 3.02 for wild-type males and 9.33 ± 3.39 for HSF2-deficient males, were not significantly different ($P = 0.997$).

Complex and multiple female fertility defects

HSF2-deficient females are hypofertile. Intercrosses of *Hsf2*$^{+/-}$ females with *Hsf2*$^{+/-}$ males resulted in 8.6 ± 2.3 offspring/litter ($n = 15$), comparable with wild-type intercrosses (8.75 ± 0.4 pups/litter; $n = 4$). In contrast, out of 17 plugged *Hsf2*$^{-/-}$ females, seven gave no offspring, five gave a normal litter and five had intermediate scores (1–4 pups), resulting in an average of 3.6 ± 3.4 pups/litter. Offspring were obtained with a similar average when *Hsf2*$^{-/-}$ females were crossed with either *Hsf2*$^{+/+}$ (2.14; $n = 7$ females) or *Hsf2*$^{-/-}$ males (3.43; $n = 7$ females) ($P = 0.52$). Thus, the reduced litter size of the *Hsf2*$^{-/-}$ females is not related to the male genotype and not due to lethality of *Hsf2*$^{-/-}$ embryos.

Increased embryonic lethality before E9.5. We examined the number and viability of the embryos at day E9.5 of gestation. Out of 11 *Hsf2*$^{-/-}$ plugged females, only five were pregnant at E9.5. The number of implanted embryos per pregnant female was normal (11.8 ± 1.3) and comparable with that observed in *Hsf2*$^{+/-}$ females (11.4; $n = 10$). However, an abnormally high number of dead embryos (resorbed or retarded) was observed (39% for *Hsf2*$^{-/-}$ females versus 18.4% for *Hsf2*$^{+/-}$ females). If considering all the plugged females, the average number of normally developing embryos at E9.5 was 3.27 ± 4.02 (instead of 9.3 for the heterozygous females) and reflected

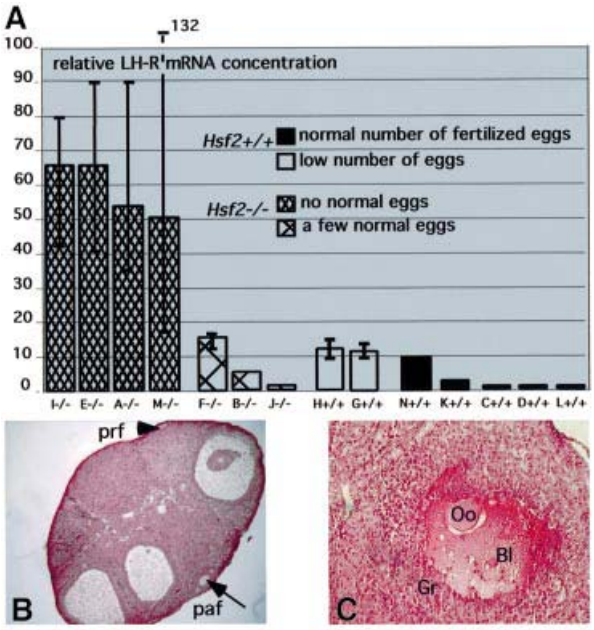

Fig. 8. Ovarian defects in *Hsf2*$^{-/-}$ females. (**A**) Abnormally elevated levels of luteinizing hormone receptor (LH-R) mRNAs in *Hsf2*$^{-/-}$ with anovulatory problems. Seven *Hsf2*$^{+/+}$ and seven *Hsf2*$^{-/-}$ 5-month-old females were mated with OF1 males. On the day of plug detection, eggs were harvested and counted in the ampulla. In parallel, LH-R mRNA levels were analyzed by RT–PCR. The relative mRNA concentration is given in arbitrary units. Value 1 was attributed to the ovary exhibiting the lowest expression level. Each plot corresponds to the average determined from three or four PCR experiments (except for female B that was tested only once). Error bars are indicated. Dense hatched bars, *Hsf2*$^{-/-}$ females that produced no eggs or only abnormal fragmented eggs. Hatched bars, *Hsf2*$^{-/-}$ females that produced a few (an average of two) fertilized eggs. Empty bars, *Hsf2*$^{+/+}$ females with no ovulated fertilized eggs. Filled bars, *Hsf2*$^{+/+}$ females with normal ovulation scores and a normal number of fertilized eggs. (**B**) Paraffin section of an *Hsf2*$^{-/-}$ ovary with marked ovulatory problems: low number of primary (prf) and pre-antral (paf) follicles. (**C**) A pre-antral hemorrhagic follicle in the section of an *Hsf2*$^{-/-}$ ovary which never gave offspring. Oo, oocyte; Gr, granulosa cells; Bl, blood.

the average of offspring/litter. It was similar at E9.5, at E16.5 (3.4 ± 4.04) and at birth (3.6 ± 3.4 pups/litter), suggesting that the majority of the defects occur before E9.5.

Ovulation defects in Hsf2$^{-/-}$ *females*. We compared the ovulation performances of nine *Hsf2*$^{-/-}$ and 10 *Hsf2*$^{+/+}$ females on the day of vaginal plug detection, after mating with wild-type outbred OF1 males. *Hsf2*$^{-/-}$ females were found to have dramatic ovulation problems. Only three *Hsf2*$^{-/-}$ females produced eggs, resulting in a total average of 3.5 eggs per *Hsf2*$^{-/-}$ female. Seven out of 10 *Hsf2*$^{+/+}$ females ovulated with a total average of 7.4 eggs per female. The average number of fertilized eggs was 0.6 fertilized egg per *Hsf2*$^{-/-}$ female versus 4.9 per *Hsf2*$^{+/+}$ female ($P < 0.05$). Indeed, *Hsf2*$^{-/-}$ females frequently produced abnormal eggs: 43.7% of the eggs were fragmented or without polar bodies (versus 5.4% for control females) or were unfertilized (40.6% with only one polar body versus 28.4% in controls).

Meiotic and hormonal problems in Hsf2$^{-/-}$ *females*. We attempted to rescue ovulation in *Hsf2*$^{-/-}$ females by administration of pregnant mare serum gonadotropin (PMSG/FSH)/human chorionic gonadotropin (hCG/LH) to 21- to 27-day-old mice, a treatment used to induce superovulation. All *Hsf2*$^{-/-}$ females were able to ovulate after this treatment. A total of 35.1 ± 22.5 eggs were ovulated by *Hsf2*$^{-/-}$ females ($n = 16$), statistically comparable ($P = 0.853$) with 37.2 ± 11.7 eggs in wild-type females ($n = 5$). However, while the eggs of wild-type females were able to develop *in vitro* to the two-cell stage with good scores (27.3 ± 1.7 eggs; 78.3% of the total ovulated eggs), eggs of *Hsf2*$^{-/-}$ females were often abnormal and only 10.2 ± 5.8 eggs (29.2% of the total) developed to the two-cell stage, which was significantly lower ($P = 0.0132$). The fact that ~70% of the eggs ovulated by *Hsf2*$^{-/-}$ females were abnormal is suggestive of meiotic problems. Since superovulation treatment rescued ovulation in *Hsf2*$^{-/-}$ females, part of the ovarian defects observed in pubescent *Hsf2*$^{-/-}$ females may be secondary to disturbed hormonal physiological concentrations of gonadotropins or ovarian function alterations.

Ovarian defects in Hsf2$^{-/-}$ *females*. To determine to what extent the ovarian function was altered, the expression level of the luteinizing hormone receptor (LH-R) was examined on the day of vaginal plug detection by semi-quantitative RT–PCR on mRNAs from individual ovaries of 5-month-old females, and their ovulation scores were determined. The level of LH-R mRNAs was found to be 50–60 times higher in the ovaries of females that ovulated no eggs or only abnormal eggs. Ovaries from *Hsf2*$^{-/-}$ females that ovulated at least a few normal eggs contained amounts of LH-R mRNAs similar to the *Hsf2*$^{+/+}$ ovaries (Figure 8A).

High LH-R mRNA levels suggested a disturbed hormonal response. Histological analysis of ovaries from *Hsf2*$^{-/-}$ females with ovulatory problems and high levels of LH-R mRNAs revealed a low number of follicles from each stage (Figure 8B). Analysis of ovaries from *Hsf2*$^{-/-}$ females that were unable to have progeny also revealed, instead of corpora lutea, the presence of hemorrhagic large follicles with a trapped oocyte (Figure 8C).

Discussion

Three main defects ensue from HSF2 deficiency in the mouse: defective meiotic chromosome synapsis and increased apoptosis in testis; female fertility problems; and altered brain morphology. Female hypofertility probably results from two apparently distinct phenomena: one related to meiotic alteration and the other having a hormone response component.

Meiosis is affected by HSF2 deficiency in males and females

Meiosis includes genetic recombination, pairing of homologous chromosomes and formation of the SC between the chromosome pairs (synapsis) (Walker and Hawley, 2000); all events that require timely controlled expression of meiotic proteins at specific developmental stages of gametogenesis.

Several lines of evidence show that meiosis is affected by HSF2 deficiency, in both males and females. Homozygous deletion of the *Hsf2* gene causes apoptosis

of nearly 25% of the cells inside the seminiferous tubules. Specifically, late pachytene and meiotically dividing spermatocytes account for almost 90% of the annexin V–FITC-positive cells, suggesting that the majority of the differentiating germ cells die in a stage-specific manner, leading to a 58% reduction in sperm count, as compared with *Hsf2*$^{+/+}$ animals. In *Hsf2*$^{-/-}$ females, meiotic defects are illustrated by a high number of abnormal eggs detected in naturally occurring ovulation or superovulation experiments. The ovaries of *Hsf2*$^{-/-}$ females with ovulatory abnormalities exhibit a lower number of follicles at each stage, and large cystic hemorrhagic follicles were observed in the ovaries of females that failed to have progeny. The high number of retarded or resorbed embryos in the litters of *Hsf2*$^{-/-}$ females, before E9.5, is suggestive of aneuploidy and consistent with meiotic disturbances.

Inactivation of a number of mammalian genes implicated in meiosis results in phenotypes similar to that of the *Hsf2*$^{-/-}$ males (Baudat *et al*., 2000; Roeder and Bailis, 2000; Romanienko and Camerini-Otero, 2000; Yuan *et al*., 2000; Tay and Richter, 2001). In these studies, meiotic problems in females were evident due to a severely reduced number of follicles in ovaries. The meiotic phenotype of *Msh5*$^{-/-}$ females is associated with estrus cycle defects and giant cysts in the ovaries, similar to that of *Hsf2*$^{-/-}$ females. *Hsf2*$^{-/-}$ ovaries therefore exhibit the stigmata of meiotic problems.

Alteration of spermatogenesis with no impact on male fertility has been reported previously. Even in cases of considerable impairment of spermatogenesis, in CPEB null mice, matings of ~20% of the CPEB null males with fertile females resulted in offspring, although the males produce six times fewer sperm than wild type and only 2% of sperm is motile (Tay and Richter, 2001).

Function of HSF2 in meiosis

Recent studies have demonstrated the existence of a 'pachytene checkpoint', the triggerring of which at late meiotic prophase leads to the elimination of defective germ cells by apoptosis (Roeder and Bailis, 2000). We observed structural defects in the SC of *Hsf2*$^{-/-}$ mice; 16.5% of the mid-pachytene spermatocytes had loop-like configurations between the lateral elements of SCs. This number is most probably an underestimate due to the limits of resolution. The lack of HSF2 may lead to disturbances in the expression of structural components of the SC or in the enzymatic activities required for synapsis/desynapsis or, alternatively, in genetic recombination preceding synapsis.

In addition to late pachytene spermatocytes, a large number of spermatocytes die at the meiotic M phase. Apoptosis may be due to premature separation of the centromere regions of the homologous chromosomes. Occasionally, we observed spermatocytes with defective synapsis at the centromere region. This is a potent mechanism for induction of unpaired univalent chromosomes that causes cell cycle arrest at the first meiotic division metaphase, which eventually leads to the elimination of arrested cells (Mahadevaiah *et al*., 2000). Alternatively, HSF2 may participate in regulation of M phase-specific molecules such as protein phosphatase 2A (PP2A) that negatively regulates entry into M phase in *Xenopus* egg extracts (Lee, 1995) and has also been implicated in regulation of microtubule dynamics and centrosome function (Snaith *et al*., 1996; Tournebize *et al*., 1997). In somatic tissue culture cells, PP2A activity has been shown to be controlled by HSF2 (Hong and Sarge, 1999).

We did not detect HSF2 in the adult ovary, but HSF2 was detected by immunohistochemistry in the primordial germ cells (data not shown). This implies that the meiotic defects in *Hsf2*$^{-/-}$ females may occur at the first meiotic division, i.e. during embryogenesis. This could explain why >43% of the ovulated eggs are fragmented or even lack the first polar body.

Hormone response disturbance in Hsf2$^{-/-}$ females

Hormonal treament of pre-pubescent females rescued a normal number of eggs ovulated in all the *Hsf2*$^{-/-}$ females. This suggests that anovulatory pubescent *Hsf2*$^{-/-}$ females naturally lack a sufficient hormonal stimulus, or do not possess an adequate ovulatory competence to respond to such a stimulus (appropriate levels of FSH- and LH-Rs). *Hsf2*$^{-/-}$ females with marked ovulatory defects exhibit abnormally elevated (50–60 times) levels of LH-Rs. Currently, we have no interpretation for these extremely high levels of LH-R mRNA, except that they are a sign of ovarian disturbance. In preliminary vaginal smear experiments, some *Hsf2*$^{-/-}$ pubescent females showed lengthening of and, later, total absence of the estrus cycle. The same females exhibited shortening of the luteal period (suggestive of non-functional corpora lutea) in pseudopregnancy experiments after mating with vasectomized males. Hypertrophy of the seminal vesicles, which was observed systematically in males, is suggestive of hormonal disturbance (Qian *et al*., 2001) and was occasionally associated with hydronephros. Whether these hormone response alterations are a consequence of the meiotic problems remains to be established. The presence of a high number of abnormal (or apoptotic) follicles due to meiotic defects in *Hsf2*$^{-/-}$ ovaries could therefore alter the dialog between follicular cells and the oocyte (Erickson and Shimasaki, 2000) and, as a consequence, the hormone response and the function of the hypothamalo-pituitary–ovarian axis. Histological analysis of pituitaries did not reveal any alterations, but HSF2 was expressed in some hypothalamic neurons, and lack of HSF2 could lead to hormone release problems.

In contrast to HSF1, necessary for the development of pre-implantation embryos (Christians *et al*., 2000) and involved in placentation (Xiao *et al*., 1999), HSF2 is dispensable for embryonic development, and *Hsf2*$^{-/-}$ females do not seem to have implantation or placentation problems. *Drosophila* HSF is necessary for oogenesis (Jedlicka *et al*., 1997), and HSF2 may have retained part of the ancestral function of this unique HSF. In *Drosophila*, Hsps are not targets of HSF during development. We could not detect significant differences between *Hsf2*$^{-/-}$ or *Hsf2*$^{+/+}$ individuals for the expression of several Hsps: HSP25, HSP84, HSP86, HSP70, GRP78, HSJ2, APG1 and APG2, by semi-quantitative RT–PCR or western blots on testis or embryonic brains. The target genes of these HSFs during development remain to be identified.

Table I. PCR primers

	Gene or RNA	PCR primers	PCR product
Southern blot probe	HSF2 (exon 4)	5′-gcgGTTTCATCTTCAAAACCAGAGG-3′ 5′-TCTGAAAGCCTGGACTCAATAG-3′	119 bp
PCR for genotyping	Primer 1 [end of intron preceding exon 5; Manuel *et al.* (1999)–beginning of exon 5 nucleotides 614–636 of the cDNA; Sarge *et al.* (1991)]	5′-GAGTGAGAATGAATCCCTTTGGAAGG-3′	
	Primer 2 (end of exon 5, nucleotides 685–689 and 16 first nucleotides of the following intron; reverse orientation)	5′-GCTGGAAGCTTCTTACCTTCCG-3′	95 bp
	Primer 3 [beginning of the *lacZ* portion of the β-*geo* gene; Kalnins *et al.* (1983)]	5′-ATGTGCTGCAAGGCGATTAAGTTGG-3′	132 bp
RT–PCR	LH receptor	5′-CTTATACATAACCACCATACCAG-3′ 5′-ATCCCAGCCACTGAGTTCATTC-3′	517 bp
	HSF2	5′-ATCCCTTTGGAAGGAGGTGT-3′ 5′-TCACAAGTTGATTATTCTGAACCAA-3′	114 bp
	Recombinant chimeric β-geo	5′-ATCCCTTTGGAAGGAGGTGT-3′ 5′-GACAGTATCGGCCTCAGGAA-3′	290 bp
	GAPDH	Xu *et al*. (1999)	300 bp
	Actin	5′-TGTTACCAACTGGGACGACA-3′ 5′-CTCTCAGCTGTGGTGAA-3′	396 bp

Brain abnormalities in Hsf2$^{-/-}$ animals

Adult *Hsf2*$^{-/-}$ mice systematically exhibit brain abnormalities characterized by the enlargement of the lateral and third ventricles. Since the choroid plexus, involved in the production of the cerebrospinal fluid, is a site of strong HSF2 expression (Figure 3A), we cannot rule out the possibility that this phenomenon is due to hydrocephaly. Since no cortex compression is observed, but rather specific reduction in the volume of hippocampus and striatum, we favor the hypothesis of a proliferative defect or an increased apoptosis rate, in agreement with HSF2 expression during embryonic life in proliferative cells of the vz. In adult brain, HSF2 was expressed in some discrete cells of the ependymal layer, which is considered as a source of stem cells in the adult brain (Momma *et al*., 2000).

Materials and methods

Construction of the targeting vector

A fragment of the *Hsf2* gene containing exon 4, the following intron and the beginning of exon 5 (Manuel *et al*., 1999) was fused in-phase with the β-*geo* gene. A further region of homology was added at the 3′ end to increase the frequency of recombination.

ES cell culture, electroporation and screening

CK35 ES cells derived from the 129/SV Pasteur strain were electroporated and selected by geneticin at 600 μg/ml (Sigma). Genomic DNA extraction and Southern blot analysis were performed as described previously (Sarig *et al*., 1999) with an external probe corresponding to exon 4, and generated by PCR (Table I).

Generation and screening of Hsf2 mutant mice

The presence of the *Hsf2* disrupted allele was detected by PCR analysis of genomic DNA on the offspring of the female chimera using a mixture of three oligonucleotides (Table I).

HSF2 detection by western blots and EMSA

Embryo extracts were prepared and western blot analysis and EMSA performed as described in Rallu *et al*. (1997). Anti-mouse HSF2 rabbit polyclonal antibody was used at a dilution of 1:10 000 (Sarge *et al*., 1993). Monoclonal antibody against HSF1 (Ab-4; Neomarkers) was used at 1:100.

Morphological analysis of the testes

Testes of wild-type and *Hsf2*$^{-/-}$ mice were isolated immediately after euthanasia by cervical dislocation. One of the two testes was fixed with Bouin's fixative at room temperature for 24 h, embedded in paraffin, cut into 5 μm sections and stained with hematoxylin and eosin. The diameter of a total of 100 tubule cross-sections was measured from five *Hsf2*$^{+/+}$ and *Hsf2*$^{-/-}$ mice. The second of the two testes was used for apoptosis and immunohistochemical assays.

Preparation and fixation of stage-specific monolayers of testicular cells

Isolation of defined stages of spermatogenesis was performed according to Parvinen and Vanha-Perttula (1972). Testes were isolated and decapsulated as described in Parvinen *et al*. (1993). For apoptosis assays and immunofluorescence, all stages of spermatogenesis were collected by cutting a short 1–3 mm segment of the seminiferous tubule from a specific stage. Segments were placed on microscope slides and covered with a coverslip to form a monolayer of cells. The squash slide was immersed in liquid nitrogen, the coverslip was removed, and the cells were fixed with ice-cold methanol:acetone (3:1) for 15 min and air dried for 60 min.

Sperm count

The epididymes of *Hsf2*$^{+/+}$ ($n = 5$) and *Hsf2*$^{-/-}$ mice ($n = 5$) were isolated, rinsed with saline solution and placed in a Petri dish containing 3 ml of M16 medium (Sigma). The sperm were released from the epididymis into the medium by applying pressure with forceps. After removal, the sperm were allowed to capacitate for 30 min before counting with a cell counter.

Apoptosis assays

Seminiferous tubules were dissociated by incubation for 30 min at 32°C with periodic agitation in Hank's balanced salt solution (HBSS) without Ca^{2+} and Mg^{2+} containing 25 mM HEPES, 1 mg/ml collagenase (type VIII; Sigma) and 1% bovine serum albumin (BSA). The tubules were dissociated by pipeting and the cell suspension was passed through a 100 μm silk membrane. Cells were centrifuged for 5 min at 500 *g* and washed with HBSS with 25 mM HEPES and 1% BSA. A 500 μl aliquot of a 1×10^6 cell suspension of fresh cells was stained with annexin V–FITC (Alexis) by mixing 500 μl of binding buffer (2.5 mM HEPES–NaOH pH 7.4, 35 mM NaCl, 0.625 mM $CaCl_2$), 2 μl of annexin V and 1 μl/ml propidium iodide (Molecular Probes) and analyzed with a FACScan flow cytometer (Becton Dickinson) using the FL1 detector at 488 nm

excitation with an argon laser. Stained cells were mixed and counted to 20 000 events. Stage-specific monolayers of testicular cells were prepared as described above and stained with annexin V–FITC using the ApoAlert kit (Clontech). TUNEL assays were performed using the Apoptag kit according to the manufacturer's instructions (Intergen Company).

Immunofluorescence and microscopy

Anti-SCP3 antibodies (a generous gift from Dr Christer Höög; Yuan *et al*., 2000) were used at 1:800 dilution. The centromere regions of meiotic chromosomes were stained with human anti-centromere sera (Crest, 1:400). A population of 500 annexin V–FITC-positive *Hsf2*$^{-/-}$ cells at early stages of apoptosis were cell cycle categorized into three groups: pachytene spermatocytes, meiotically dividing spermatocytes or other cell type. A total of 200 mid-pachytene cells were scored for SC defects in five *Hsf2*$^{+/+}$ and five *Hsf2*$^{-/-}$ mice.

Statistical analysis

Student's *t*-test was used with 95% confidence interval.

Superovulation experiments and in vitro culture of one-cell stage embryos

Superovulation experiments and egg recovery from ampulla were performed as described (Hogan *et al*., 1994). *In vitro* culture of one-cell stage embryos was performed at 37°C by incubation in M16 medium (Sigma).

β-galactosidase staining and histological analysis

Whole embryos were fixed in 4% paraformaldehyde (PFA) in phosphate-buffered saline (PBS). Pre-implantation embryos were fixed in 0.2% glutaraldehyde; 2% PFA. Frozen sections (16 µm) of the X-gal-stained E7.5 embryos were performed after cryoprotection of the embryos in 15% sucrose and 7% gelatin (Merck 1.04070 Mikrobiologie). X-gal-stained E13.5 embryos (Sarig *et al*., 1999) were sectioned by vibratome (200 µm) after embedding in gelatin/ovalbumin (0.5%; 30%). For adult animals, testes were fixed in 4% PFA after removal of the tunica albicans and soft tearing of the seminiferous tubules. X-gal-stained testes were embedded in paraffin and cut in 10 µm sections which were counterstained with eosin. Adult mice were perfused through the heart with 4% PFA for 20 min, dissected brains were sectioned by vibratome after embedding in gelatin/ovalbumin, and the 200 µm sections were stained with X-gal. Ovaries were fixed in Bouin fixative and embedded in paraffin, then cut in 6 µm sections on a microtome and stained with hematoxylin and eosin.

HSF2 immunocytochemistry

Paraffin (10 µm) or frozen (50 µm) sections of immersion-fixed neural tubes were incubated with anti-HSF2 polyclonal antibodies (Fiorenza *et al*., 1995) at 1:300–1:100 dilutions (Rallu *et al*., 1997).

BrdU labeling

BrdU (20 mg/kg) was injected intraperitoneally at E12.5 and E15.5, and pregnant females were sacrificed 2 or 3 h after. BrdU staining was carried out as described in Takahashi *et al*. (1992) on 50 µm frozen sections of immersion-fixed neural tubes at both stages.

Semi-quantitative RT–PCR and RT–PCR detection of HSF2

Total RNA was isolated from ovaries by using Trizol reagent (Life Technologies). A 2 µg aliquot of total RNA and 1 µg of oligo(dT) primers (Promega) were annealed. Reverse transcription was carried out with M-MLV reverse transcriptase as described by the manufacturer (Life Technologies). Aliquots of 0.5 µl and 4-fold serial dilutions were used in a 25 µl PCR mixture containing 200 µM of each deoxynucleotide (Promega), 500 nM of each primer, 2.5 µl of 10× Expand HF buffer with 15 mM $MgCl_2$, and 0.87 U of Expand High Fidelity enzyme mix (Roche). PCR conditions were 94°C for 5 min, then 94°C for 45 s, 61°C for 1 min, 72°C for 45 s for 23–25 cycles and 72°C for 7 min.

An 18 µl aliquot of the reaction was run on a 1% agarose gel in 1× TBE and photographed on a UV transilluminator using a digital camera. The relative levels of mRNAs in different samples were determined by quantitating the intensity of the ethidium bromide-stained bands using NIH Image, and calculating the fold dilution of the starting material that would be required to obtain similar signal intensities.

Primers used for the molecular characterization of the *Hsf2* KO are described in Table I.

Acknowledgements

We thank Dr Philippe Soriano for the gift of plasmid pSAβgeo, Jacqueline Barra and Charles Babinet for injecting the recombinant ES clones, Yvan Lallemand for help in the first breeding of mice, Nadine Binart and Aurélie Lucas for advice on LH receptor detection, Christer Höög for kindly providing the anti-SCP3 antibody, Henri Blomster, Andrey Mikhailov, Thomas Söderström and Cindy Lasnier for technical help, and Michael Dresser for discussions and critical comments on the manuscript. The work was supported by grants to L.S. from The Academy of Finland, The Sigrid Juselius Foundation and The Finnish Cancer Organizations, and grants to M.M. and V.M. (nos 9293 and 5939) and a fellowship to M.M. from the Association pour la Recherche sur le Cancer. T.-P.A. was supported by The Turku Graduate School of Biomedical Sciences and Y.C. by the Association Franco-Chinoise pour la Recherche Scientifique et Technique and the French Embassy in China.

References

Alastalo,T.P., Lonnstrom,M., Leppa,S., Kaarniranta,K., Pelto-Huikko,M., Sistonen,L. and Parvinen,M. (1998) Stage-specific expression and cellular localization of the heat shock factor 2 isoforms in the rat seminiferous epithelium. *Exp. Cell Res.*, **240**, 16–27.

Baudat,F., Manova,K., Pui Yuen,J., Jasin,M. and Keeney,S. (2000) Chromosone synapsis defects and sexually dimorphic meiotic progression in mice lacking Spo11. *Mol. Cell*, **6**, 989–998.

Christians,E., Michel,E., Adenot,P., Mezger,V., Rallu,M., Morange,M. and Renard,J.P. (1997) Evidence for the involvement of mouse heat shock factor 1 in the atypical expression of hsp70.1 heat shock gene during mouse zygotic genome activation. *Mol. Cell. Biol.*, **17**, 778–788.

Christians,E., Davis,A.A., Thomas,S.D. and Benjamin,I.J. (2000) Maternal effect of *Hsf1* on reproductive success. *Nature*, **407**, 693–694.

Clermont,Y. (1972) Kinetics of spermatogenesis in mammals: seminiferous epithelium cycle and spermatogonia renewal. *Physiol. Rev.*, **52**, 198–236.

Eddy,E.M. (1999) Role of heat shock protein HSP70-2 in spermatogenesis. *Rev. Reprod.*, **4**, 23–30.

Erickson,G.F. and Shimasaki,S. (2000) The role of the oocyte in folliculogenesis. *Trends Endocrinol. Metab.*, **11**, 193–198.

Fiorenza,M.T., Farkas,T., Dissing,M., Kolding,D. and Zimarino,V. (1995) Complex expression of murine heat shock transcription factors. *Nucleic Acids Res.*, **23**, 467–474.

Friedrich,G. and Soriano,P. (1991) Promoter traps in embryonic stem cells: a genetic screen to identify and mutate developmental genes in mice. *Genes Dev.*, **5**, 1513–1523.

Henriksen,K. and Parvinen,M. (1998) Stage-specific apoptosis of male germ cells in the rat: mechanism of cell death studied by supravital squash preparations. *Tissue Cell*, **30**, 692–701.

Hogan,B., Beddington,R., Costantini,F. and Lucy,E. (1994) *Manipulating the Mouse Embryo. A Laboratory Manual*, 2nd edn. Cold Spring Harbor Laboratory Press, Cold Spring Harbor, NY, pp. 131–132.

Hong,Y. and Sarge,K.D. (1999) Regulation of protein phosphatase 2A activity by heat shock transcription factor 2. *J. Biol. Chem.*, **274**, 12967–12970.

Jedlicka,P., Mortin,M.A. and Wu,C. (1997) Multiple functions of *Drosophila* heat shock transcription factor *in vivo*. *EMBO J.*, **16**, 2452–2462.

Kalnins,A., Otto,K., Rüther,U. and Müller-Hill,B. (1983) Sequence of the *lacZ* gene of *Escherichia coli*. *EMBO J.*, **2**, 593–597.

Lee,T.H. (1995) The role of protein phosphatase type-2A in the *Xenopus* cell cycle: initiation of the G_2/M transition. *Semin. Cancer Biol.*, **6**, 203–209.

Mahadevaiah,S.K., Evans,E.P. and Burgoyne,P.S. (2000) An analysis of meiotic impairment and of sex chromosome associations throughout meiosis in XYY mice. *Cytogenet. Cell Genet.*, **89**, 29–37.

Manuel,M., Sage,J., Mattei,M., Morange,M. and Mezger,V. (1999) Genomic structure and chromosomal localization of the mouse *Hsf2* gene and promoter sequences. *Gene*, **232**, 115–124.

Mathew,A. and Morimoto,R.I. (1998) Role of the heat-shock response in the life and death of proteins. *Ann. N. Y. Acad. Sci.*, **851**, 99–111.

McMillan,D.R., Xiao,X., Shao,L., Graves,K. and Benjamin,I.J. (1998) Targeted disruption of heat shock transcription factor 1 abolishes

thermotolerance and protection against heat-inducible apoptosis. *J. Biol. Chem.*, **273**, 7523–7528.
Mezger,V., Rallu,M., Morimoto,R.I., Morange,M. and Renard,J.P. (1994a) Heat shock factor 2-like activity in mouse blastocysts. *Dev. Biol.*, **166**, 819–822.
Mezger,V., Renard,J.P., Christians,E. and Morange,M. (1994b) Detection of heat shock element-binding activities by gel shift assay during mouse preimplantation development. *Dev. Biol.*, **165**, 627–638.
Momma,S., Johansson,C.B. and Frisen,J. (2000) Get to know your stem cells. *Curr. Opin. Neurobiol.*, **10**, 45–49.
Nakai,A., Suzuki,M. and Tanabe,M. (2000) Arrest of spermatogenesis in mice expressing an active heat shock transcription factor 1. *EMBO J.*, **19**, 1545–1554.
Parvinen,M. and Vanha-Perttula,T. (1972) Identification and enzyme quantitation of the stages of the seminiferous epithelial wave in the rat. *Anat. Rec.*, **174**, 435–449.
Parvinen,M., Toppari,J. and Lähdetie,J. (1993) Transillumination phase contrast microscopic techniques for evaluation of male germ cell toxicity and mutagenicity. In Chapin,R.E. and Heindel,J.J. (eds), *Methods in Toxicology*, 3. Academic Press, New York, NY, pp. 142–165.
Pirkkala,L., Nykänen,P. and Sistonen,L. (2001) Roles of the heat shock transcription factors in regulation of the heat shock response and beyond. *FASEB J.*, **15**, 1118–1131.
Qian,Y.M., Sun,X.J., Tong,M.H., Li,X.P. and Richa Song,W. (2001) Targeted disruption of the mouse estrogen sulfotransferase gene reveals a role of estrogen metabolism in intracrine and paracrine estrogen regulation. *Endocrinology*, **142**, 5342–5350.
Rallu,M., Loones,M., Lallemand,Y., Morimoto,R., Morange,M. and Mezger,V. (1997) Function and regulation of heat shock factor 2 during mouse embryogenesis. *Proc. Natl Acad. Sci. USA*, **94**, 2392–2397.
Roeder,G.S. and Bailis,J.M. (2000) The pachytene checkpoint. *Trends Genet.*, **16**, 395–403.
Romanienko,P.J. and Camerini-Otero,R.D. (2000) The mouse Spo11 gene is required for meiotic chromosome synapsis. *Mol. Cell*, **6**, 975–987.
Sarge,K.D., Zimarino,V., Holm,K., Wu,C. and Morimoto,R.I. (1991) Cloning and characterization of two mouse heat shock factors with distinct inducible and constitutive DNA-binding ability. *Genes Dev.*, **5**, 1902–1911.
Sarge,K.D., Murphy,S.P. and Morimoto,R.I. (1993) Activation of heat shock gene transcription by heat shock factor 1 involves oligomerization, acquisition of DNA-binding activity and nuclear localization and can occur in the absence of stress. *Mol. Cell. Biol.*, **13**, 1392–1407.
Sarge,K.D., Park-Sarge,O.K., Kirby,J.D., Mayo,K.E. and Morimoto,R.I. (1994) Expression of heat shock factor 2 in mouse testis: potential role as a regulator of heat-shock protein gene expression during spermatogenesis. *Biol. Reprod.*, **50**, 1334–1343.
Sarig,R., Mezger-Lallemand,V., Gitelman,I., Davis,C., Fuchs,O., Yaffe,D. and Nudel,U. (1999) Targeted inactivation of Dp71, the major non-muscle product of the DMD gene: differential activity of the Dp71 promoter during development. *Hum. Mol. Genet.*, **8**, 1–10.
Schalk,J.A., Dietrich,A.J., Vink,A.C., Offenberg,H.H., van Aalderen,M. and Heyting,C. (1998) Localization of SCP2 and SCP3 protein molecules within synaptonemal complexes of the rat. *Chromosoma*, **107**, 540–548.
Sheldon,L.A. and Kingston,R.E. (1993) Hydrophobic coiled-coil domains regulate the subcellular localization of human heat shock factor 2 [published erratum appears in *Genes Dev*., 1994, **8**, 386]. *Genes Dev.*, **7**, 1549–1558.
Snaith,H.A., Armstrong,C.G., Guo,Y., Kaiser,K. and Cohen,P.T. (1996) Deficiency of protein phosphatase 2A uncouples the nuclear and centrosome cycles and prevents attachment of microtubules to the kinetochore in *Drosophila* microtubule star (mts) embryos. *J. Cell Sci.*, **109**, 3001–3012.
Takahashi,T., Nowaskowski,R.S. and Caviness,V.S. (1992) BrdU as an S-phase marker for quantitative studies of cytokinetic behaviour in the murine cerebral ventricular zone. *J. Neurocytol.*, **21**, 185–197.
Tay,J. and Richter,J.D. (2001) Germ cell differentiation and synaptonemal complex formation are disrupted in CPEB knockout mice. *Dev. Cell*, **1**, 201–213.
Tournebize,R., Andersen,S.S., Verde,F., Doree,M., Karsenti,E. and Hyman,A.A. (1997) Distinct roles of PP1 and PP2A-like phosphatases in control of microtubule dynamics during mitosis. *EMBO J.*, **16**, 5537–5549.
van Engeland,M., Nieland,L.J., Ramaekers,F.C., Schutte,B. and Reutelingsperger,C.P. (1998) Annexin V-affinity assay: a review on an apoptosis detection system based on phosphatidylserine exposure. *Cytometry*, **31**, 1–9.
Vermes,I., Haanen,C., Steffens-Nakken,H. and Reutelingsperger,C. (1995) A novel assay for apoptosis. Flow cytometric detection of phosphatidylserine expression on early apoptotic cells using fluorescein labelled annexin V. *J. Immunol. Methods*, **184**, 39–51.
Voss,A.K., Thomas,T. and Gruss,P. (2000) Mice lacking HSP90β fail to develop a placental labyrinth. *Development*, **127**, 1–11.
Walker,M.Y. and Hawley,R.S. (2000) Hanging on to your homolog: the roles of pairing, synapsis and recombination in the maintenance of homolog adhesion. *Chromosoma*, **109**, 3–9.
Wu,C. (1995) Heat shock transcription factors: structure and regulation. *Annu. Rev. Cell Dev. Biol.*, **11**, 441–469.
Xiao,X., Davis,A.A., McMillan,D.R., Zuo,X.X., Curry,B.B., Richardson,J.A. and Benjamin,I.J. (1999) Growth retardation, female infertility, placental insufficiency and susceptibility to endotoxemia in mice lacking HSF1. *EMBO J.*, **18**, 5943–5952.
Xu,C., Liguori,G., Persico,M.G. and Adamson,E.D. (1999) Abrogation of the *Cripto* gene in mouse leads to failure of postgastrulation morphogenesis and lack of differentiation of cardiomyocytes. *Development*, **126**, 483–494.
Yuan,L., Liu,J.-G., Zhao,J., Brundell,E., Daneholt,B. and Höög,C. (2000) The murine SCP3 gene is required for synaptonemal complex assembly, chromosome synapsis and male fertility. *Mol. Cell*, **65**, 73–83.

Received January 15, 2002; revised March 20, 2002; accepted April 4, 2002